THE JOURNAL OF PHYSICAL CHEMISTRY LETTERS
A JOURNAL OF THE AMERICAN CHEMICAL SOCIETY

pubs.acs.org/JPCL

Letter

Effect of Surface Functionalization on the Magnetization of Fe_3O_4 Nanoparticles by Hybrid Density Functional Theory Calculations

Enrico Bianchetti and Cristiana Di Valentin*

Cite This: *J. Phys. Chem. Lett.* 2022, 13, 9348−9354

Read Online

ACCESS | Metrics & More | Article Recommendations | Supporting Information

ABSTRACT: Surface functionalization is found to prevent the reduction of saturation magnetization in magnetite nanoparticles, but the underlying mechanism is still to be clarified. Through a wide set of hybrid density functional theory (HSE06) calculations on Fe_3O_4 nanocubes, we explore the effects of the adsorption of various ligands (containing hydroxyl, carboxylic, phosphonic, catechol, and silanetriol groups), commonly used to anchor surfactants during synthesis or other species during chemical reactions, onto the spin and structural disorder, which contributes to the lowering of the nanoparticle magnetization. The spin-canting is simulated through a spin-flip process at octahedral Fe ions and correlated with the energy separation between O^{2-} 2p and Fe^{3+}_{Oct} 3d states. Only multidentate bridging ligands hamper the spin-canting process by establishing additional electronic channels between octahedral Fe ions for an enhanced ferromagnetic superexchange interaction. The presence of anchoring organic acids also interferes with structural disorder, by disfavoring surface reconstruction.

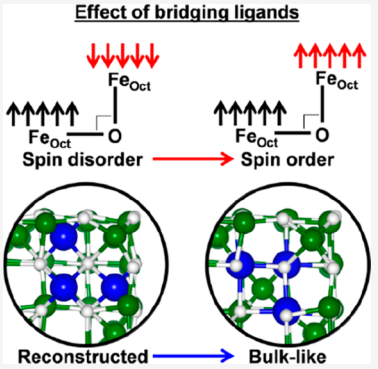

Magnetite is the mineral with the highest iron content and with the most intense magnetic properties existing in nature. The inverse spinel crystal structure of $Fe(II)Fe(III)_2O_4$ presents O anions in a face-centered cubic arrangement with the Fe(II) ions in octahedral sites, and the Fe(III) ions half in octahedral and half in tetrahedral sites. The net ferrimagnetic ordering (4.1 μ_B per unit formula)[1] results from the superexchange interaction between the Fe cations through the O anions, which is antiferromagnetic (AFM) for $Fe_{oct}-O-Fe_{tet}$ whereas it is ferromagnetic (FM) for $Fe_{oct}-O-Fe_{oct}$.[2,3] The saturation magnetization of bulk magnetite is 96 emu/g.

Magnetite nanoparticles (NPs) can be prepared with different sizes and shapes through controlled synthetic routes[4−9] and are used in various medical applications as contrast agents for magnetic resonance imaging, in magnetic hyperthermia, or as drug carriers,[10−14] after being clinically tested and approved for commercialization.

However, the magnetic properties of NPs are not as excellent as those of bulk magnetite, with a saturation magnetization that is largely reduced due to a combination of several contributing factors. The three, generally recognized, main causes of reduced magnetization are the presence of antiphase domains,[15,16] a low degree of crystallinity, and surface spin-canting effects.[17,18]

Although NPs larger than 80 nm size are usually multidomain,[19,20] there is still controversy on the minimum size of NPs where multidomains can coexist, depending on the synthetic route or preparation conditions.[16] In the present work, we will not address this aspect for two reasons: first, because there is reasonable expectation that very small NPs (<25 nm), such as those that are typically used in nanomedical applications, are homogeneously magnetized and are stable single domain;[21] second, because it has been already theoretically investigated in terms of Heisenberg spin Hamiltonian or through density functional theory with the Hubbard U correction (DFT+U) calculations.[16,22]

A loss in crystallinity at the surface layers has been often invoked as a cause of reduced saturation magnetization in NPs. It is well-known that even extended Fe_3O_4 (001) surfaces, which constitute the most stable type of magnetite surface,[23−25] spontaneously reconstruct through an atomic reorganization where a loss in Fe:O stoichiometry is accompanied by the transfer of some subsurface octahedral Fe ions from the third layer into tetrahedral sites in the second layer.[26] Indeed, we have shown in a previous study by some of us that a similar reconstruction takes place at the corners of cubic magnetite NPs.[27] This NP shape is one of the most commonly observed[28] and is enclosed by six (001) facets.[5,7] Here, similarly, octahedral Fe ions around the corner move into tetrahedral sites causing structural disorder. However, these surface reconstructions could be hampered using capping agents during NP crystal growth, such as oleic acid, which is often used during NP preparation. However, no theoretical

Received: July 13, 2022
Accepted: September 28, 2022
Published: October 3, 2022

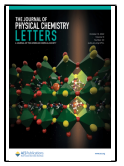

https://doi.org/10.1021/acs.jpclett.2c02186
J. Phys. Chem. Lett. 2022, 13, 9348−9354

simulations have yet effectively proven this ability of coating polymers to enhance the surface crystallinity of NPs.

Coated magnetic NPs were indeed found to present much higher saturation magnetization, almost close to the bulk value, than naked ones, e.g., 84 vs 46 emu/g.[29−31] A possible explanation, besides the reduced reconstruction, is that surface coating interferes with spin-canting phenomena, but why and how it could improve the alignment of surface atom spins with the overall magnetization direction of the NP is still a big open question, especially because the covering organic acids are not magnetic. In a recent work,[32] based on hybrid density functional theory (DFT) calculations on a model of a cubic NP, we have shown that the high saturation magnetization observed for magnetic NPs coated with carboxylic acids is not just simply due to a higher crystallinity of the sample or a reduced disorder at the surface, but it is the consequence of a direct involvement of the carboxylic group in the mechanism of spin alignments. This anchoring functional group bridges pairs of Fe surface ions and becomes involved in a ferromagnetic superexchange interaction between them, which is the reason for the enhanced magnetization with respect to naked NPs but in analogy with the bulk magnetite situation. To corroborate this analysis, based on delicate spin-flipping calculations, we compared the results with those for a nonbridging but still O containing anchoring group, i.e., the hydroxyl group.[33] Indeed, no ferromagnetic superexchange effect was observed in this case.

Since magnetic NPs are not just coated with hydrophobic organic acids, but eventually those are substituted after synthesis through a "grafting to" approach with many other interesting ligands for a stronger or more efficient surface functionalization,[14] here we are going to investigate whether the effect that we have observed for the bridging carboxylate group is unique or could be triggered also by other Fe-bridging anchoring groups. If our hypothesis proves true, the protecting polymeric shell not only would provide Fe_3O_4 NPs with enhanced dispersion and long-term stability in biological media, together with the possibility of attaching therapeutic agents or targeting agents,[13,14,33] but also could be used well to improve the magnetic properties by proper tailoring of the grafting strategy.

In the present study we use the protocol developed in our previous work,[32] based on hybrid DFT calculations, and we apply it comparatively to several different and commonly used anchoring ligands: carboxylic group, phosphonic group, catechol, and silanetriol.[14,33] At the end of this study, we will also address the role played by the ligands on the NP surface reconstruction.

The hybrid DFT method used is HSE06[34] because it was proven to reliably reproduce magnetic properties of bulk, surface, and nanostructures of Fe_3O_4.[27,35,36] Further details on the computational setup are provided in the Supporting Information and in refs 27, 35, and 36. The magnetite NP model used in the present study is cubic, is made of 429 atoms, and is enclosed by six (001) facets, as observed in the experiments for the most popular cubic NPs.[5,7] Such cubic nanostructures were observed to undergo surface reconstruction at four of the eight corners, i.e., those exposing tetrahedral Fe atoms (see Figure 1), from here on referred to as Fe-corner (note that the other four expose O atoms, from here on referred to as O-corner).[27] Ligand coating for spin-flip calculations is modeled at two different local coverages: low and high. The local low coverage is characterized by one single adsorbed ligand, whereas the local high coverage is by three adsorbed ligands, in the proximity of the Fe ion under investigation. Local high coverage was already proved to well represent the effect of full coverage (when all surface Fe sites are covered by ligands) on spin-flip properties.[32] Ligand coating for surface reconstruction calculations is modeled at full coverage. The total magnetization is computed according to the formula:[27]

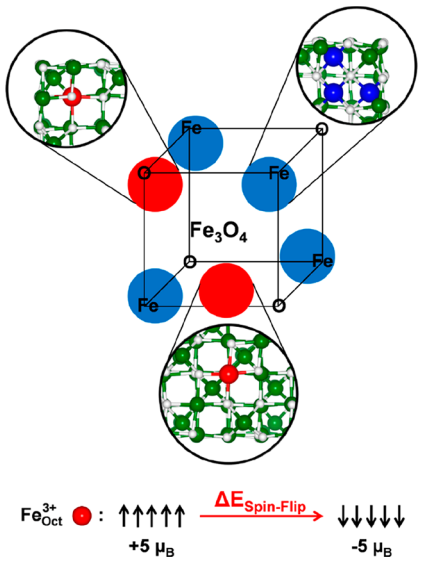

Figure 1. Structural scheme of the magnetite cubic NP. The red circles indicate the corner and the surface portion where the spin-flip process, schematized at the bottom of the figure, is investigated. The blue circles indicate the corners involved in the reconstruction process. The ball-and-stick insets show the details of the surroundings of Fe atoms that are involved in the spin-flip (red beads, which are Fe^{3+}_{Oct}6*c*-(**3**) in the corner and Fe^{3+}_{Oct}5*c*-(**5**) on the flat surface, according to the labels used in Figure S1 and in ref 32) and reconstruction process (blue beads). The white and green beads represent O and Fe.

$$m_{tot} = 5 \times [N(Fe^{3+}_{Oct}) - N(Fe^{3+}_{Tet})] + 4 \times [N(Fe^{2+}_{Oct}) - N(Fe^{2+}_{Tet})] \quad (1)$$

where Fe^{3+}_{Oct} and Fe^{2+}_{Oct} are Fe^{3+} and Fe^{2+} ions at octahedral sites, Fe^{3+}_{Tet} and Fe^{2+}_{Tet} are Fe^{3+} and Fe^{2+} ions at tetrahedral sites, and N is the number of the corresponding ions.

We mimic the spin disorder, or spin-canting, phenomena by inducing a spin-flip from +5 μ_B to −5 μ_B on specific Fe^{3+}_{Oct} ions[32,37] (as schematically described on bottom of Figure 1) in the corner and on the flat surface, which are named Fe^{3+}_{Oct}6*c*-(**3**) and Fe^{3+}_{Oct}5*c*-(**5**) according to the labels used in Figure S1 and in our previous work,[32] respectively, as described in Figure 1 and in the corresponding caption. These two specific Fe sites are chosen because the first is a special Fe ion in the proximity of the O-corner, whereas the second is a superficial Fe ion on one of the flat facets. On naked NPs, we have observed in our previous work[32] that the spin-flip at Fe^{3+}_{Oct}6*c*-(**3**), followed by atomic relaxation, is characterized by a very tiny energy cost $\Delta E_{SF+Rel} = \Delta E_{Spin-Flip} + \Delta E_{Relaxation}$ = +13 meV), and therefore, we expect it can easily take place at room temperature (Table 1). On the flat facet at the Fe^{3+}_{Oct}5*c*-(**5**) site, the cost is 10 times larger (+137 meV in Table 1) and, therefore, unfeasible at room temperature.[32]

https://doi.org/10.1021/acs.jpclett.2c02186
J. Phys. Chem. Lett. 2022, 13, 9348−9354

Table 1. Selected Nanoparticle Fe^{3+}_{Oct} Sites Considered for the Spin-Flip Mechanism Investigation[a]

	coverage	AA	MPA	CAT	SIL	ETH
Fe^{3+}_{Oct}6c-(3)	naked			+13[b] (+270[b])		
	low	−49[b] (+80[b])	−10 (+16)	−27 (+4)	−33 (−1)	−39 (−8)
	high	+141[b] (+165[b])	+120 (+130)	+118 (+131)	+134 (+143)	−15[b] (+15)
Fe^{3+}_{Oct}5c-(5)	naked			+137[b] (+208[b])		
	high	+280 (+310)	+241 (+275)	+219 (+257)	+209 (+248)	+114 (+210)

[a]The ΔE_{SF+Rel} and ΔE_{SF} (inside the parentheses) values are reported in meV for different ligands at different coverages. [b]These values are taken from ref 32.

In contrast, when the NP is decorated with acetic acid (AA) at a high local coverage regime (see Figure 2 and Figure S2),

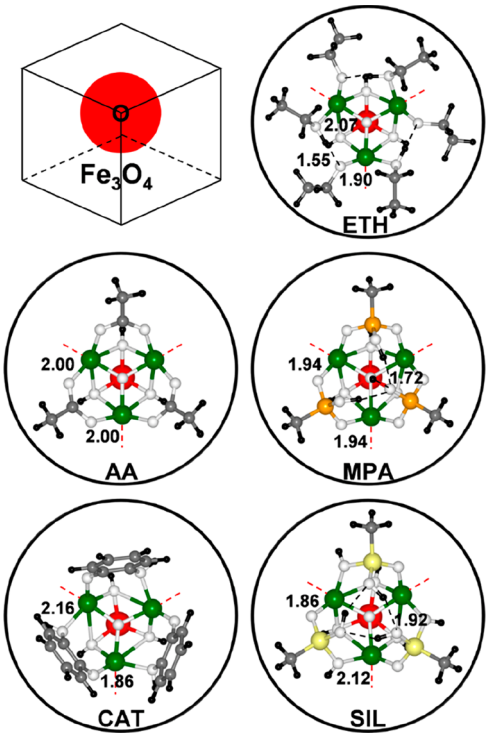

Figure 2. Ball-and-stick representations for the adsorption of different ligands at local high coverage onto the NP corner. Only the ligands and the NP O-corner are shown for clarity, as schematized in the top left corner of the figure. The red dashed lines indicate the edges of the hidden NP. The black dashed lines indicate the formation of hydrogen bonds. The H-bond and the Fe−O_{Ligand} bond lengths (in Å) for the asymmetric unit are shown. The black, gray, orange, yellow, white, green, and red beads represent H, C, P, Si, O, Fe, and Fe_{Oct} on which the spin-flip process is investigated, respectively.

we have observed that the spin-flip process is unfavorable on both Fe^{3+}_{Oct}6c-(3) and Fe^{3+}_{Oct}5c-(5) and it is accompanied by a small relaxation energy (ΔE_{SF+Rel} = +141[32] and +280 meV, respectively, see Table 1). As already mentioned in the introduction, the effect of the presence of acetic acid at a high density is related to the ability of this bridging ligand to reconnect several surface octahedral Fe ions and, thus, induce an extra FM superexchange effect. To corroborate this, we also considered a ligand that is not bridging, i.e., ethanol (ETH in Figure 2, dissociating similarly to water molecules[38,39]), and we confirmed that in this case spin-flipping is still an easy process at Fe^{3+}_{Oct}6c-(3), as observed for naked NPs (−15 meV vs +13 meV, respectively, as reported in Table 1).[32]

As a further step, we now present the results for other bridging anchoring ligands, starting from phosphonic acid. In particular, we considered methylphosphonic acid (MPA), as the simplest prototypical molecule, in several adsorption modes (see Figure S3 and Figure S4): undissociated monodentate, dissociated chelate, undissociated bidentate, dissociated bidentate, and bidissociated bidentate. The most stable configuration at the O-corner, in the low coverage regime, is the bidissociated bidentate, with an adsorption energy of −5.71 eV (see Figure S3, Figure S4, and Table 2),

Table 2. Adsorption Energies (in eV per molecule) for Different Ligands at Different Coverages onto the NP

E_{ads}(eV/molecule)	AA	MPA	CAT	SIL	ETH
corner−low coverage	−2.98[a]	−5.71	−3.91	−4.62	−2.32
corner−high coverage	−3.00	−3.85	−2.66	−3.00	−1.60
surface−high coverage	−2.44	−3.66	−2.55	−2.92	−1.57

[a]This value is taken from ref 32.

which is at least 1 eV larger than those computed for the other modes. Note that one of the two dissociated protons goes on the extremely reactive O atom at the O-corner, causing some Fe−O bond breaking and corner reconstruction, whereas the other is adsorbed on an O atom of the flat surface that is generally recognized in the literature as the most easily protonated.[40,41] If we increase the local density of MPA molecules at the O-corner, in the proximity of the Fe^{3+}_{Oct}6c-(3) site (Figure 2), using the three undercoordinated octahedral Fe ions around the O at the vertex, the additional two MPA molecule are found to preferentially adsorb as monodissociated bidentate, which is one of the most common adsorption modes on metal oxide surfaces.[42] The presence of the other two MPA molecules prevents the Fe−O bond breaking at the O-corner upon OH formation. We also considered MPA adsorption on flat 001 facets, around the Fe^{3+}_{Oct}5c-(5) site, with two MPA molecules (Figure S2) in the dissociated bidentate mode (−3.66 eV per molecule).

The spin-flipping accompanied by atomic relaxation at Fe^{3+}_{Oct}6c-(3) and Fe^{3+}_{Oct}5c-(5) sites, when local high coverage of MPA is reached, is clearly much less favorable than for the naked NP, similarly to what observed in the presence of high density of AA: +120 meV and +241 meV, for the two sites, respectively, vs +141 and +280 for AA. Therefore, the bridging ligand MPA [O−P−O], similar to AA [O−C−O], is perfectly capable of activating additional superexchange interaction among octahedral Fe ions.

Next, we consider catechol-based ligands, which are well-known to stably anchor metal oxide surfaces. Again, catechol (CAT) is a bridging ligand [O−C−C−O] that can attach to two surface cations in a bidentate fashion. Indeed, the monodissociated bidentate adsorption mode is found to be

https://doi.org/10.1021/acs.jpclett.2c02186
J. Phys. Chem. Lett. 2022, 13, 9348−9354

that with the largest adsorption energy (−3.91 eV) at the O-corner site (see Table 2, Figure S3, and Figure S5), if compared to undissociated bidentate, bidissociated bidentate, undissociated chelate, dissociated chelate, and bidissociated chelate, which are at least 1 eV higher in energy if not unstable. When three CAT molecules are anchored to the O-corner by using the three octahedral Fe ions around the O at the vertex, we observe a highly symmetric structure, as shown in Figure 2. On the flat 001 facets, catechol molecules are similarly monodissociated and bidentate as on the corner sites (Figure S2).

It is not so easily predictable whether the [O−C−C−O] bridge will be effective in inducing magnetic communication between Fe ions. The results confirm that, in the presence of a high coverage of CAT ligands, spin-flipping, even accompanied by atomic relaxation, is a hampered process by +118 meV at the Fe^{3+}_{Oct}6*c*-(**3**) site and by 219 meV at the Fe^{3+}_{Oct}5*c*-(**5**) site. These numbers are slightly smaller than for AA and MPA but are still very close.

The last class of anchoring ligand we have investigated is based on a silanetriol group. In particular, we have considered methylsilanetriol (SIL), which consists of three [O−Si−O] bridges. Similarly to MPA, this ligand could potentially be tridentate; however, it is found to be bidentate because the (001) magnetite surface presents superficial Fe rows that are too distant to allow the tridentation. Here, we observe that at the O-corner SIL is preferentially monodissociated and bidentate on two undercoodinated octahedral Fe ions next to the O at the vertex (see Figure S6), both at low (−4.62 eV) and high (−3.00 eV) coverage densities (see Figure S3 and Figure 2, respectively). We considered other absorption modes, which are at least half an eV higher in energy: undissociated bidentate, bidissociated bidentate, and dissociated chelate.

Are the [O−Si−O] bridges affective for superexchange interaction among octahedral Fe ions? The answer is again positive with an energy cost for spin-flipping, even allowing atomic relaxation, of +134 meV at the Fe^{3+}_{Oct}6*c*-(**3**) site and by 209 meV at the Fe^{3+}_{Oct}5*c*-(**5**) site, in line with the other bridging anchoring ligands considered in this study (see Table 1 for direct comparison).

The calculations clearly suggest that all bidentate bridging ligands induce an extra FM superexchange interaction between octahedral Fe ions, which reinforces the overall magnetization of the NPs and suppresses spin disorder phenomena. This effect is evaluated in terms of energy cost (ΔE_{SF+Rel}) to induce spin-flip and corresponding atomic relaxation on an octahedral Fe ion in the proximity of the O-corner, where spin and structural reorganization can more easily take place. Larger values of ΔE_{SF+Rel} reflect larger magnetic exchange coupling constants (J) between octahedral Fe ions. To understand the origin of this extra FM superexchange, we have analyzed the dependency of J with the variation of the O^{2-} 2p band energy levels with respect to the Fe^{3+}_{Oct} 3d ones (Δ_{pd}), according to the formula:[43]

$$J \propto \frac{2t_{pd}^4}{(U_d + \Delta_{pd})^2} \quad (2)$$

where t_{pd} is the hopping integral between p and d orbitals, and U_d is the Coulomb repulsion between two electrons in a d orbital, respectively. Similarly to what done in our previous work,[32] the charge transfer energy Δ_{pd} is estimated as the energy difference between the center of mass (COM) of the O^{2-} 2p-band and of the Fe^{3+}_{Oct} 3d-band, as detailed in the SI. Since we simulated a local high coverage of ligands at the O-corner, only the spin-flipping Fe site, Fe^{3+}_{Oct}6*c*-(**3**), and the O and Fe atoms in its first and second coordination sphere, are considered in the calculation of the O^{2-} p-band and the Fe^{3+}_{Oct} d-band COM. We compute a Δ_{pd} of 2.05 eV for the naked NP and of 1.55, 1.49, 1.54, and 1.60 eV for the NP at high coverage of AA, MPA, CAT, and SIL, respectively. According to eq 2, a reduction of Δ_{pd} (here of about 0.5 eV) is expected to enhance the magnetic exchange coupling constant, in perfect agreement with the increase in spin-flip energy cost observed in our calculations, as schematized in Figure 3. This

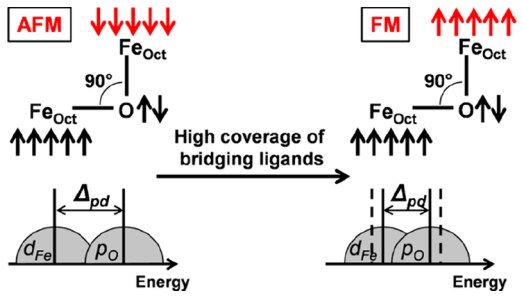

Figure 3. Schematic representation of the extra ferromagnetic (FM) superexchange interaction between octahedral Fe ions induce by adsorbed bridging ligands.

analysis is corroborated also by the opposite case of a local high coverage of ETH, for which we compute a Δ_{pd} value very close to that for the naked NP (1.98 eV vs 2.05 eV, respectively), confirming no additional FM exchange, as suggested by the ΔE_{SF+Rel} value (−15 meV[32]) in favor of spin-flipping.

Based on these results and analysis, we can state that an induced extra FM superexchange effect among Fe_{oct} sites in the surface layers is only triggered by adsorption of a bridging ligand that electronically connects different Fe_{oct} sites, such as acetate, phosphonate, catechol, and silanetriol derivates but not monocoordinated molecules, such as ethanol. We further proved this concept by calculating the monodentate AA at local high coverage, as shown in Figure S7. Indeed, we obtain a tiny energy cost of 47 meV for ΔE_{SF+Rel}, confirming a cheap spin-flip process, in contrast with what is observed for the bidentate (bridging) mode whose ΔE_{SF+Rel} is three times larger.

In this last paragraph, we wish to get some insight into the role played by ligands on the NP surface reconstruction, since this is one of the major factors affecting the saturation magnetization of NPs, together with spin-canting and the presence of antiphase domain boundaries. In a previous study by some of us,[27] we have proved that bulk-like cubic NPs are stabilized by surface reconstruction, which consists of the transfer of six-coordinated iron atoms near an Fe-corner from octahedral to tetrahedral sites (see Figure 1). Such an atomic reconstruction was found to reduce the total magnetization of the NP by 9.7% (from 1232 μ_B to 1112 μ_B). In the present study, we have found out that this type of reconstruction stabilizes the cubic NP model under investigation by −10.6 eV. At the top of Figure 4, we show the naked NP before (bulk-like, left) and after (reconstructed, right) the atomic reconstruction, which involves three octahedral iron atoms

https://doi.org/10.1021/acs.jpclett.2c02186
J. Phys. Chem. Lett. 2022, 13, 9348−9354

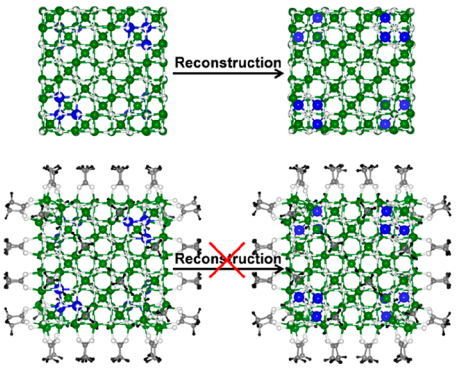

Figure 4. Ball-and-stick representations of the minimum energy structures of the unreconstructed (left) and reconstructed (right) nanoparticle in the absence (top) and in the presence (down) of the acetic acid molecules at full coverage. The black, gray, white, green, and blue beads represent H, C, O, Fe, and Fe_{Oct} which are involved in the reconstruction process, respectively.

(blue beads in the image) for each Fe-corner (four out of a total of eight corners per cube). However, if the NP is fully decorated by the organic ligands (AA), we note that the reconstructed model is less stable than the bulk-like one by 7.4 eV (Figure 4, the bottom). We also considered half coverage (see Figure S8), but this is not sufficient to lift the reconstruction. Thus, only high coverage organic acid coating can reverse the energetics with respect to what is observed for the naked NPs, largely stabilizing the bulk-like structure whose total magnetic moment is by far higher than that of the reconstructed NP (408 μ_B versus 288 μ_B, respectively). This finding is in line with what was found by means of surface X-ray diffraction, infrared spectroscopy, and DFT+U calculations by Arndt and collaborators for the (001) surface,[44] i.e., that the adsorption of organic acid reverses the reconstruction process of the (001) surface, through the stabilization of the bulk-like structure and formation of deep bulk Fe vacancies.[44] Furthermore, this result suggests that using coating agents during the synthesis of the nanostructures is a successful strategy to prepare NPs with high saturation magnetization, close to the bulk value.

In summary, in this Letter we have shed light on the underlying reasons why surface functionalization of NPs keeps saturation magnetization values close to those of the bulk. Not only carboxylic groups, commonly used to anchor surfactants (e.g., oleic acid) during NPs synthesis, but also other kinds of multidentate bridging anchoring groups, which can exchange with surfactants after the synthesis, are found to create electronic channels through chemical bridges between Fe_{oct} sites that induce an extra ferromagnetic superexchange interaction, and work against spin-flipping processes and, consequently, also against the reduction of the total magnetic moments observed for noncoated NPs. Our conclusion is corroborated by the fact that coating with monodentate ligands does not lead to such behavior. In the last part of this Letter, we also show that surface functionalization by organic acids prevents crystallinity loss in NPs, which again improves their total magnetic moment. This is because the surface reconstruction, consisting of octahedral Fe ions that move into tetrahedral sites, is found not to be energetically favorable in the presence of the coating molecules.

To conclude, the results of this computational study provide a first-principles description, at the electronic and atomistic level, of the mechanisms regarding how surface functionalization alters the spin and structural disorder (spin-canting and atomic reconstruction) in magnetite NPs and, consequently, affects their saturation magnetization. Since this specific physical property is crucial for an efficacious nanomedical application, the concepts developed here can be useful to guide the design and preparation of optimal magnetite-based nanostructures.

■ ASSOCIATED CONTENT

Supporting Information

The Supporting Information is available free of charge at https://pubs.acs.org/doi/10.1021/acs.jpclett.2c02186.

Further computational details, global minimum energy structure of the magnetite cubic nanoparticle, figures describing the adsorption of different ligands at local high (low) coverage onto the nanoparticle surface (corner), figures describing the different adsorption modes tested for each ligand, figure of the bulk-like and reconstructed nanoparticles at half acetic acid coverage, and further details regarding the spin-flip of Fe_{Oct} in the naked NP case (PDF)

■ AUTHOR INFORMATION

Corresponding Author

Cristiana Di Valentin − *Dipartimento di Scienza dei Materiali, Università di Milano Bicocca, 20125 Milano, Italy; BioNanoMedicine Center NANOMIB, Università di Milano Bicocca, 20900 Monza, Italy;* orcid.org/0000-0003-4163-8062; Email: cristiana.divalentin@unimib.it

Author

Enrico Bianchetti − *Dipartimento di Scienza dei Materiali, Università di Milano Bicocca, 20125 Milano, Italy*

Complete contact information is available at: https://pubs.acs.org/10.1021/acs.jpclett.2c02186

Notes

The authors declare no competing financial interest.

■ ACKNOWLEDGMENTS

The authors are grateful to Lorenzo Ferraro for his technical help and to Hongsheng Liu for useful discussions. The project has received funding from the European Research Council (ERC) under the European Union's HORIZON2020 research and innovation programme (ERC Grant Agreement [647020]).

■ REFERENCES

(1) Banerjee, S. K.; Moskowitz, B. M.Ferrimagnetic properties of magnetite. In *Magnetite Biomineralization and Magnetoreception in Organisms, a New Biomagnetism*; Kirschvink, J. L., Jones, D. S., MacFadden, B. J., Eds.; Springer: New York, 1985.

(2) Goodenough, J. B.; Loeb, A. L. Theory of ionic ordering, crystal distortion, and magnetic exchange due to covalent forces in spinels. *Phys. Rev.* **1955**, *98* (2), 391.

(3) Goodenough, J. B.*Magnetism and the Chemical Bond*; Wiley Interscience: New York, 1963.

(4) Park, J.; An, K.; Hwang, Y.; Park, J. G.; Noh, H. J.; Kim, J. Y.; Park, J. H.; Hwang, N. M.; Hyeon, T. Ultra-large-scale syntheses of monodisperse nanocrystals. *Nat. Mater.* **2004**, *3* (12), 891−895.

(5) Kovalenko, M. V.; Bodnarchuk, M. I.; Lechner, R. T.; Hesser, G.; Schäffler, F.; Heiss, W. Fatty acid salts as stabilizers in size-and shape-

controlled nanocrystal synthesis: the case of inverse spinel iron oxide. *J. Am. Chem. Soc.* **2007**, *129* (20), 6352−6353.
(6) Zhao, L.; Zhang, H.; Xing, Y.; Song, S.; Yu, S.; Shi, W.; Guo, X.; Yang, J.; Lei, Y.; Cao, F. Morphology-controlled synthesis of magnetites with nanoporous structures and excellent magnetic properties. *Chem. Mater.* **2008**, *20* (1), 198−204.
(7) Kim, D.; Lee, N.; Park, M.; Kim, B. H.; An, K.; Hyeon, T. Synthesis of uniform ferrimagnetic magnetite nanocubes. *J. Am. Chem. Soc.* **2009**, *131* (2), 454−455.
(8) Zhao, L.; Duan, L. Uniform Fe_3O_4 octahedra with tunable edge length-synthesis by a facile polyol route and magnetic properties. *Eur. J. Inorg. Chem.* **2010**, *2010*, 5635−5639.
(9) Li, X.; Liu, D.; Song, S.; Wang, X.; Ge, X.; Zhang, H. Rhombic dodecahedral Fe_3O_4: ionic liquid-modulated and microwave-assisted synthesis and their magnetic properties. *CrystEngComm* **2011**, *13* (20), 6017−6020.
(10) Pankhurst, Q. A.; Connolly, J.; Jones, S. K.; Dobson, J. Applications of magnetic nanoparticles in biomedicine. *J. Phys. D: Appl. Phys.* **2003**, *36* (13), R167−R181.
(11) Gupta, A. K.; Gupta, M. Synthesis and surface engineering of iron oxide nanoparticles for biomedical applications. *Biomaterials* **2005**, *26* (18), 3995−4021.
(12) Colombo, M.; Carregal-Romero, S.; Casula, M. F.; Gutiérrez, L.; Morales, M. P.; Böhm, I. B.; Heverhagen, J. T.; Prosperi, D.; Parak, W. J. Biological applications of magnetic nanoparticles. *Chem. Soc. Rev.* **2012**, *41* (11), 4306−4334.
(13) Wu, W.; Jiang, C. Z.; Roy, V. A. Designed synthesis and surface engineering strategies of magnetic iron oxide nanoparticles for biomedical applications. *Nanoscale* **2016**, *8* (47), 19421−19474.
(14) Hou, Z.; Liu, Y.; Xu, J.; Zhu, J. Surface engineering of magnetic iron oxide nanoparticles by polymer grafting: synthesis progress and biomedical applications. *Nanoscale* **2020**, *12* (28), 14957−14975.
(15) Margulies, D. T.; Parker, F. T.; Rudee, M. L.; Spada, F. E.; Chapman, J. N.; Aitchison, P. R.; Berkowitz, A. E. Origin of the anomalous magnetic behavior in single crystal Fe_3O_4 films. *Phys. Rev. Lett.* **1997**, *79* (25), 5162.
(16) Nedelkoski, Z.; Kepaptsoglou, D.; Lari, L.; Wen, T.; Booth, R. A.; Oberdick, S. D.; Galindo, P. L.; Ramasse, Q. M.; Evans, R. F. L.; Majetich, S.; Lazarov, V. K. Origin of reduced magnetization and domain formation in small magnetite nanoparticles. *Sci. Rep.* **2017**, *7* (1), 45997.
(17) Martinez, B.; Obradors, X.; Balcells, L.; Rouanet, A.; Monty, C. Low temperature surface spin-glass transition in γ-Fe_2O_3 nanoparticles. *Phys. Rev. Lett.* **1998**, *80* (1), 181.
(18) Baaziz, W.; Pichon, B. P.; Fleutot, S.; Liu, Y.; Lefevre, C.; Greneche, J. M.; Toumi, M.; Mhiri, T.; Begin-Colin, S. Magnetic iron oxide nanoparticles: reproducible tuning of the size and nanosized-dependent composition, defects, and spin canting. *J. Phys. Chem. C* **2014**, *118* (7), 3795−3810.
(19) Dunlop, D. J.; Özdemir, O.*Rock Magnetism: Fundamentals and Frontiers*; Cambridge University Press: Cambridge, 1997.
(20) Krishnan, K. M.; Pakhomov, A. B.; Bao, Y.; Blomqvist, P.; Chun, Y.; Gonzales, M.; Griffin, K.; Ji, X.; Roberts, B. K. Nanomagnetism and spin electronics: materials, microstructure and novel properties. *J. Mater. Sci.* **2006**, *41* (3), 793−815.
(21) Reichel, V.; Kovács, A.; Kumari, M.; Bereczk-Tompa, É.; Schneck, E.; Diehle, P.; Posfai, M.; Hirt, A. M.; Duchamp, M.; Dunin-Borkowski, R. E.; Faivre, D. Single crystalline superstructured stable single domain magnetite nanoparticles. *Sci. Rep.* **2017**, *7* (1), 45484.
(22) McKenna, K. P.; Hofer, F.; Gilks, D.; Lazarov, V. K.; Chen, C.; Wang, Z.; Ikuhara, Y. Atomic-scale structure and properties of highly stable antiphase boundary defects in Fe_3O_4. *Nat. Commun.* **2014**, *5* (1), 5740.
(23) Santos-Carballal, D.; Roldan, A.; Grau-Crespo, R.; de Leeuw, N. H. A DFT study of the structures, stabilities and redox behaviour of the major surfaces of magnetite Fe_3O_4. *Phys. Chem. Chem. Phys.* **2014**, *16* (39), 21082−21097.
(24) Parkinson, G. S. Iron oxide surfaces. *Surf. Sci. Rep.* **2016**, *71* (1), 272−365.
(25) Feld, A.; Weimer, A.; Kornowski, A.; Winckelmans, N.; Merkl, J. P.; Kloust, H.; Zierold, R.; Schmidtke, C.; Schotten, T.; Riedner, M.; Bals, S.; Weller, H. Chemistry of shape-controlled iron oxide nanocrystal formation. *ACS Nano* **2019**, *13* (1), 152−162.
(26) Bliem, R.; McDermott, E.; Ferstl, P.; Setvin, M.; Gamba, O.; Pavelec, J.; Schneider, M. A.; Schmid, M.; Diebold, U.; Blaha, P.; Hammer, L.; Parkinson, G. S. Subsurface cation vacancy stabilization of the magnetite (001) surface. *Science* **2014**, *346* (6214), 1215−1218.
(27) Liu, H.; Di Valentin, C. Shaping magnetite nanoparticles from first principles. *Phys. Rev. Lett.* **2019**, *123* (18), 186101.
(28) Roca, A. G.; Gutierrez, L.; Gavilan, H.; Fortes Brollo, M. E.; Veintemillas-Verdaguer, S.; Morales, M. d. P. Design strategies for shape-controlled magnetic iron oxide nanoparticles. *Adv. Drug Delivery Rev.* **2019**, *138*, 68−104.
(29) Daou, T. J.; Grenèche, J. M.; Pourroy, G.; Buathong, S.; Derory, A.; Ulhaq-Bouillet, C.; Donnio, B.; Guillon, D.; Begin-Colin, S. Coupling agent effect on magnetic properties of functionalized magnetite-based nanoparticles. *Chem. Mater.* **2008**, *20* (18), 5869−5875.
(30) Roca, A. G.; Niznansky, D.; Poltierova-Vejpravova, J.; Bittova, B.; González-Fernández, M. A.; Serna, C. J.; Morales, M. P. Magnetite nanoparticles with no surface spin canting. *J. Appl. Phys.* **2009**, *105* (11), 114309.
(31) Salafranca, J.; Gazquez, J.; Perez, N.; Labarta, A.; Pantelides, S. T.; Pennycook, S. J.; Batlle, X.; Varela, M. Surfactant organic molecules restore magnetism in metal-oxide nanoparticle surfaces. *Nano Lett.* **2012**, *12* (5), 2499−2503.
(32) Bianchetti, E.; Di Valentin, C. Mechanism of spin ordering in Fe_3O_4 nanoparticles by surface coating with organic acids. *Mater. Today Nano* **2022**, *17*, 100169.
(33) Heuer-Jungemann, A.; Feliu, N.; Bakaimi, I.; Hamaly, M.; Alkilany, A.; Chakraborty, I.; Masood, A.; Casula, M. F.; Kostopoulou, A.; Oh, E.; Susumu, K.; Stewart, M. H.; Medintz, I. L.; Stratakis, E.; Parak, W. J.; Kanaras, A. G. The role of ligands in the chemical synthesis and applications of inorganic nanoparticles. *Chem. Rev.* **2019**, *119* (8), 4819−4880.
(34) Krukau, A. V.; Vydrov, O. A.; Izmaylov, A. F.; Scuseria, G. E. Influence of the exchange screening parameter on the performance of screened hybrid functionals. *J. Chem. Phys.* **2006**, *125* (22), 224106.
(35) Liu, H.; Di Valentin, C. Band gap in magnetite above Verwey temperature induced by symmetry breaking. *J. Phys. Chem. C* **2017**, *121* (46), 25736−25742.
(36) Liu, H.; Di Valentin, C. Bulk-terminated or reconstructed Fe_3O_4(001) surface: Water makes a difference. *Nanoscale* **2018**, *10* (23), 11021−11027.
(37) Herng, T. S.; Xiao, W.; Poh, S. M.; He, F.; Sutarto, R.; Zhu, X.; Li, R.; Yin, X.; Diao, C.; Yang, Y.; Huang, X.; Yu, X.; Feng, Y. P.; Rusydi, A.; Ding, J. Achieving a high magnetization in sub-nanostructured magnetite films by spin-flipping of tetrahedral Fe^{3+} cations. *Nano Res.* **2015**, *8* (9), 2935−2945.
(38) Meier, M.; Hulva, J.; Jakub, Z.; Pavelec, J.; Setvin, M.; Bliem, R.; Schmid, M.; Diebold, U.; Franchini, C.; Parkinson, G. S. Water agglomerates on Fe_3O_4(001). *Proc. Natl. Acad. Sci. U. S. A.* **2018**, *115* (25), E5642−E5650.
(39) Righi, G.; Fabris, S.; Piccinin, S. Oxygen evolution reaction on the Fe_3O_4(001) surface: theoretical insights into the role of terminal and bridging oxygen atoms. *J. Phys. Chem. C* **2021**, *125* (34), 18752−18761.
(40) Parkinson, G. S.; Mulakaluri, N.; Losovyj, Y.; Jacobson, P.; Pentcheva, R.; Diebold, U. Semiconductor-half metal transition at the Fe_3O_4(001) surface upon hydrogen adsorption. *Phys. Rev. B* **2010**, *82* (12), 125413.
(41) Bourgund, A.; Lechner, B. A.; Meier, M.; Franchini, C.; Parkinson, G. S.; Heiz, U.; Esch, F. Influence of local defects on the dynamics of O-H bond breaking and formation on a magnetite surface. *J. Phys. Chem. C* **2019**, *123* (32), 19742−19747.
(42) Guerrero, G.; Alauzun, J. G.; Granier, M.; Laurencin, D.; Mutin, P. H. Phosphonate coupling molecules for the control of

https://doi.org/10.1021/acs.jpclett.2c02186
J. Phys. Chem. Lett. 2022, 13, 9348−9354

surface/interface properties and the synthesis of nanomaterials. *Dalton Trans.* **2013**, *42* (35), 12569−12585.
(43) Koch, E. Exchange Mechanisms. In *The Physics of Correlated Insulators, Metals, and Superconductors*; Pavarini, E., Koch, E., Scalettar, R., Martin, R., Eds.; Forschungszentrum Jülich: Jülich, 2017.
(44) Arndt, B.; Sellschopp, K.; Creutzburg, M.; Granas, E.; Krausert, K.; Vonk, V.; Muller, S.; Noei, H.; Feldbauer, G. B. V.; Stierle, A. Carboxylic acid induced near-surface restructuring of a magnetite surface. *Commun. Chem.* **2019**, *2*, 92.

https://doi.org/10.1021/acs.jpclett.2c02186
J. Phys. Chem. Lett. 2022, 13, 9348−9354